ADVANCED ENERGY MATERIALS

Supporting Information

for *Adv. Energy Mater.,* DOI: 10.1002/aenm.202203284

Double Paddle-Wheel Enhanced Sodium Ion Conduction in an Antiperovskite Solid Electrolyte

*Ping-Chun Tsai, Sunil Mair, Jeffrey Smith, David M. Halat, Po-Hsiu Chien, Kwangnam Kim, Duhan Zhang, Yiliang Li, Liang Yin, Jue Liu, Saul H. Lapidus, Jeffrey A. Reimer, Nitash P. Balsara, Donald J. Siegel, and Yet-Ming Chiang**

Double-Paddle-Wheel Enhanced Sodium Ion Conduction in an Antiperovskite Solid Electrolyte, Supplementary Information

Ping-Chun Tsai,[1] Sunil Mair,[2] Jeffrey Smith,[3] David M. Halat,[4] Po-Hsiu Chien,[5] Kwangnam Kim,[3] Duhan Zhang,[2] Yiliang Li,[2] Liang Yin,[6] Jue Liu,[5] Saul H. Lapidus,[6] Jeffrey A. Reimer,[4] Nitash P. Balsara,[4] Donald J. Siegel,[7] and Yet-Ming Chiang[2]

[1]*National Taiwan University of Science and Technology*, [2]*Massachusetts Institute of Technology*, [3]*University of Michigan, Ann Arbor*, [4]*University of California, Berkeley*, [5]*Oakridge National Laboratory*, [6]*Argonne National Laboratory*, [7]*University of Texas at Austin*

Physical Characterization of $Na_{3-x}O_{1-x}(NH_2)_x(BH_4)$

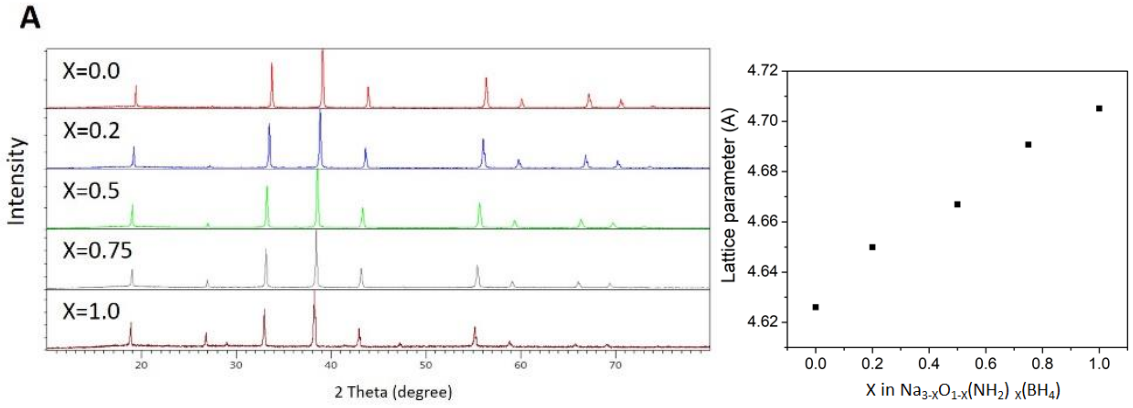

Figure S1. (A) PXRD patterns show that all as-synthesized $Na_{3-x}O_{1-x}(NH_2)_x(BH_4)$ compositions form a cubic AP with space group *Pm*-3*m* and Rietveld refinement phase purity of > 99 wt%. The trace impurities were identified as excess reactants. (B) The lattice parameters increase linearly with increasing *x* in $Na_{3-x}O_{1-x}(NH_2)_x(BH_4)$, indicating the formation of a solid-solution phase. The lattice parameters for the two endmember compositions of $Na_3O(BH_4)$ and $Na_2(NH_2)(BH_4)$, are 4.63 Å and 4.71 Å respectively, a change of 1.7%.

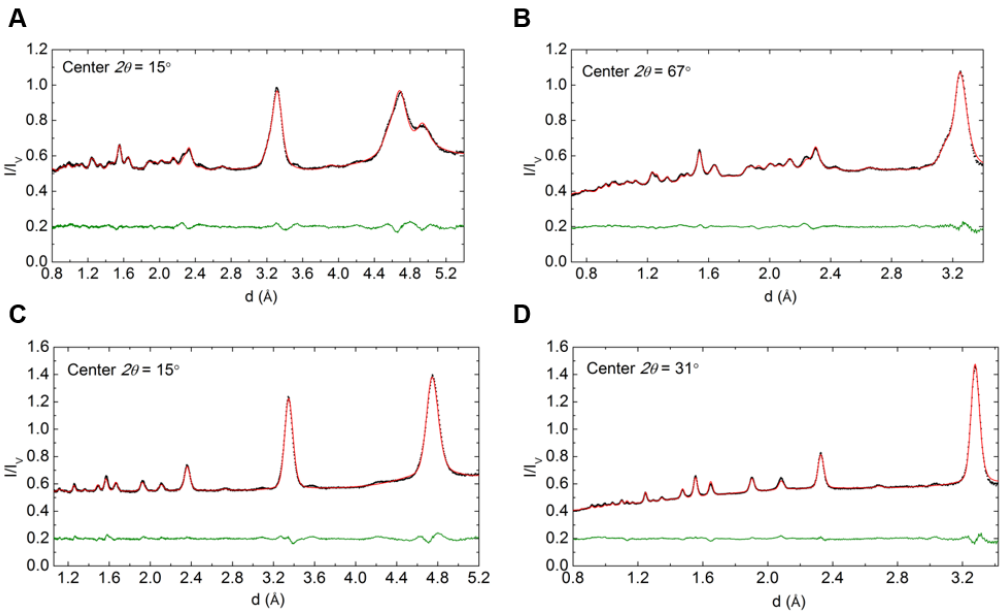

Figure S2. Refinement results of $Na_2NH_2BD_4$ using neutron diffraction data at (A, B) 100 K and (C, D) 288 K. Experimental data is shown in black, the refined model in red, and the difference curve in green.

Electrical Characterization

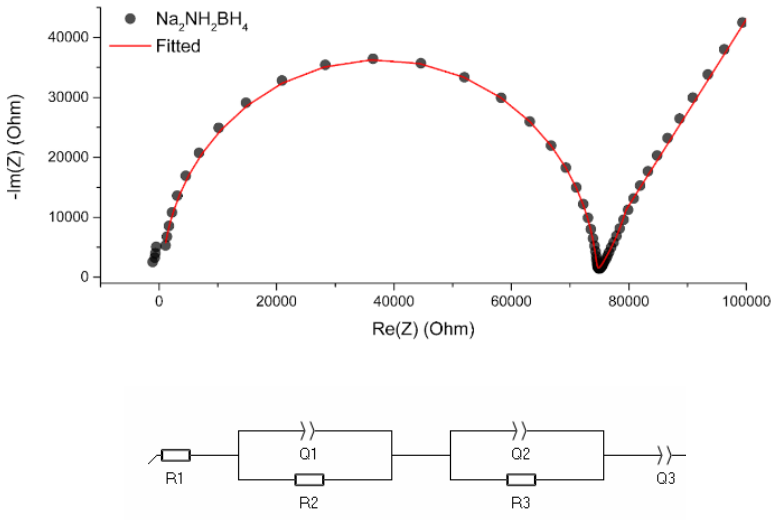

Figure S3. (A) Representative Nyquist plot of EIS data and model fit. (B) Equivalent circuit model used for fitting (R1: wire and equipment resistance, R2: grain resistance, Q1: grain capacitance, R3: grain boundary resistance, Q2: grain boundary capacitance), typically only one arc was observed. Circuit fitting deviation ±5Ω.

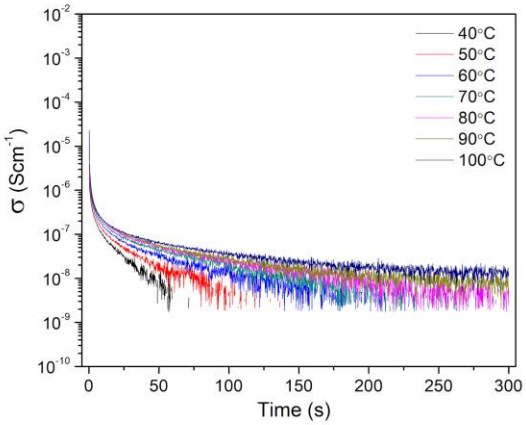

Figure S4. Constant voltage hold (100 mV) DC measurements using gold blocking electrodes for temperatures between 40 and 100 °C. The resultant current measurement is converted to electrical conductivity based on the sample area and thickness. Electrical conductivity was found to be negligible relative to ionic conductivity.

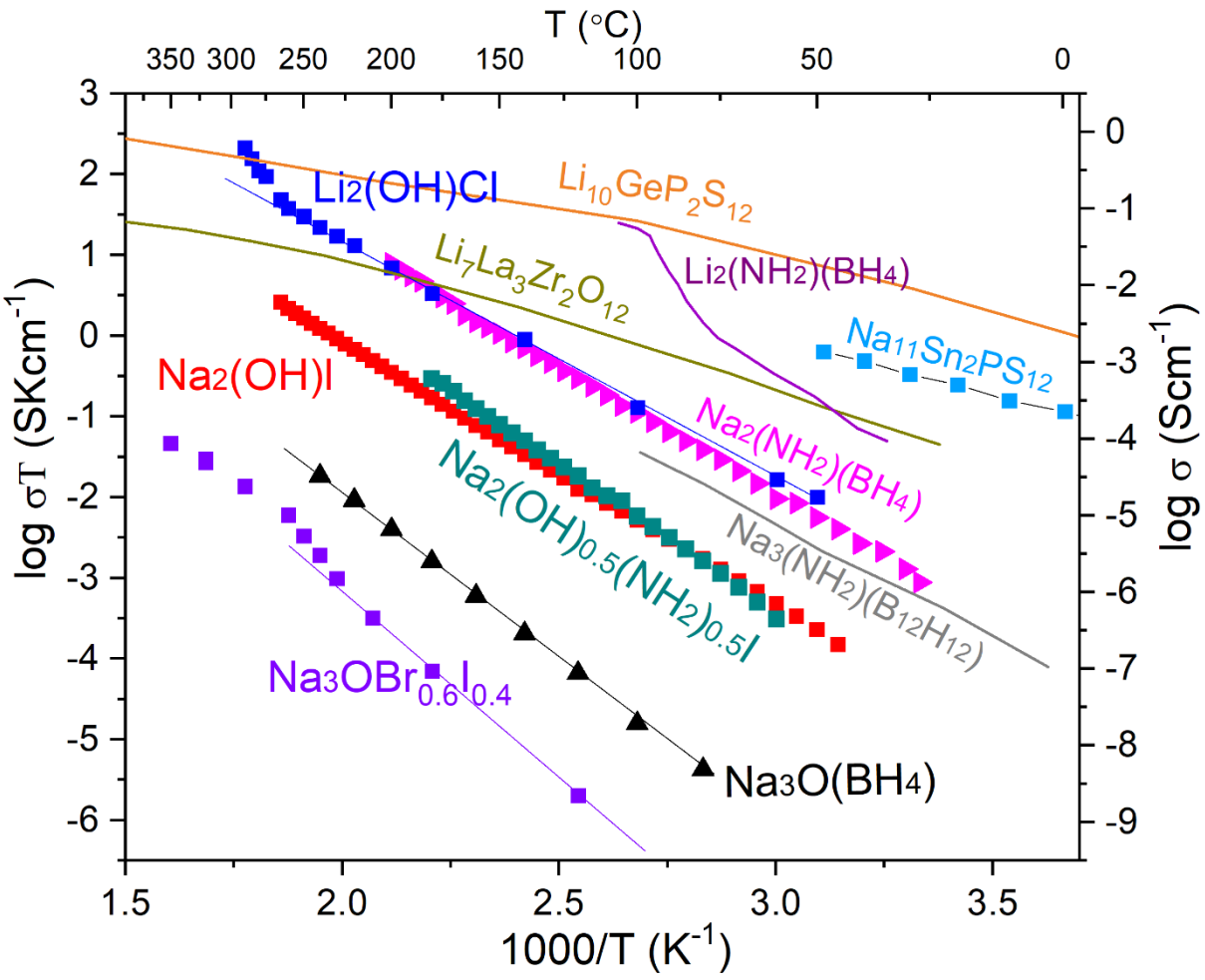

Figure S5. Ionic conductivities for various sodium antiperovskite compounds compared to literature results for several well-known solid-state electrolytes. Results for $Na_3OBr_{0.6}I_{0.4}$, $Na_3O(BH_4)$, $Na_2(OH)_{0.5}(NH2)_{0.5}I$, $Na_2(OH)I$, $Na_2(NH_2)(BH_4)$ were measured in the present work.

AIMD Results

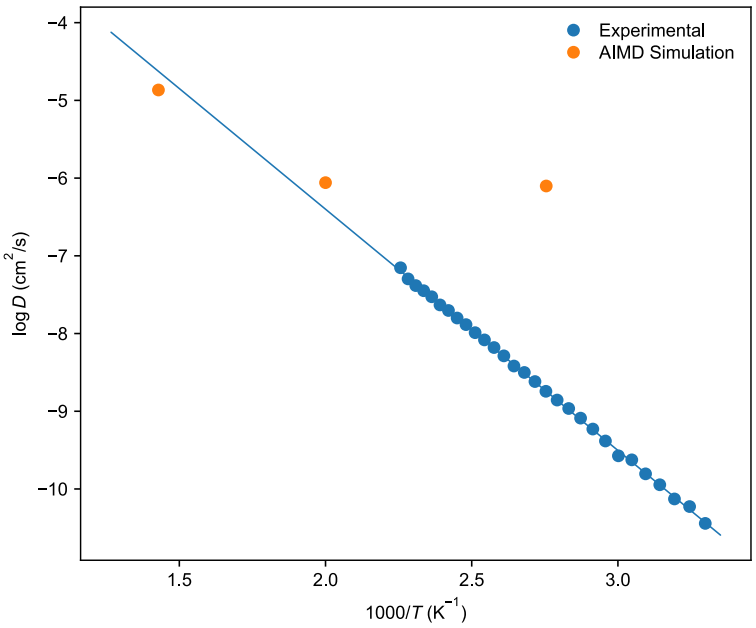

Figure S6. Sodium diffusivity values calculated from AIMD simulations of $Na_2(NH_2)(BH_4)$ at 363, 500, and 700 K compared to experimental data from EIS between 300 and 450 K. Theory and experiment agree well at the higher temperatures (500 and 700 K), but due to timescale limitations and slower dynamics at low temperatures, the AIMD data at 363 K likely does not produce an accurate measure of diffusivity.

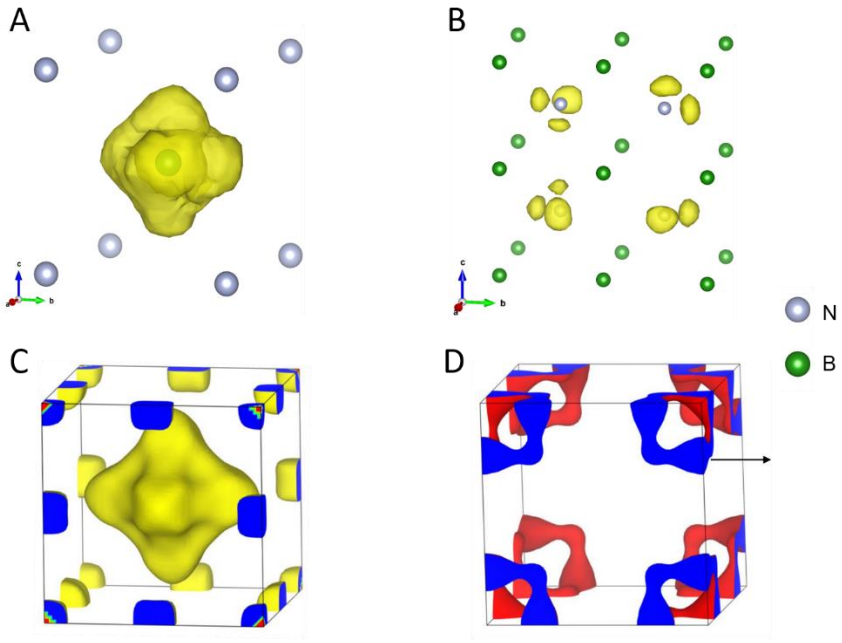

Figure S7. Probability density iso-surfaces from an AIMD simulation of $Na_2(NH_2)(BH_4)$ at 300 K for (A) hydrogen surrounding boron in BH_4^- (2×10^{-5} a.u. iso-surface level) and (B) hydrogen surrounding nitrogen in NH_2^- (1×10^{-4} a.u. iso-surface level) alongside MEM analysis of neutron diffraction data of $Na_2(NH_2)(^{11}BD_4)$ at 295 K for (C) deuterium surrounding boron in $^{11}BD_4^-$ and (D) hydrogen surrounding nitrogen in NH_2^-. Due to timescale limitations and slower dynamics at 300 K, the slower-rotating NH_2^- units in the AIMD simulation (panel B) do not each explore all preferred orientations. Nevertheless, when the iso-surfaces of the four NH_2^- units are combined, they result in an isotropic surface that matches well with the MEM analysis (panel D). Furthermore, the better agreement between theory and experiment for the BH_4^- units (panels A and C) reflects their faster rotation, which allows them to sample more orientations within the simulated timescale.

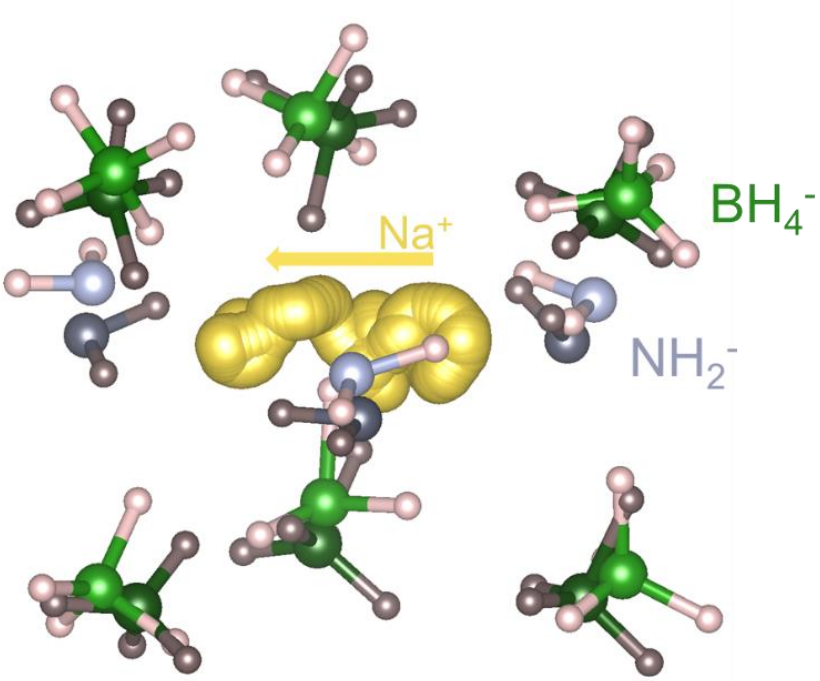

Figure S8. Atomic trajectories for the representative migration event analyzed in Figure 4. Every frame is shown for the sodium ion, while for the neighboring cluster anions just the initial and final positions are shown (dark and light respectively).

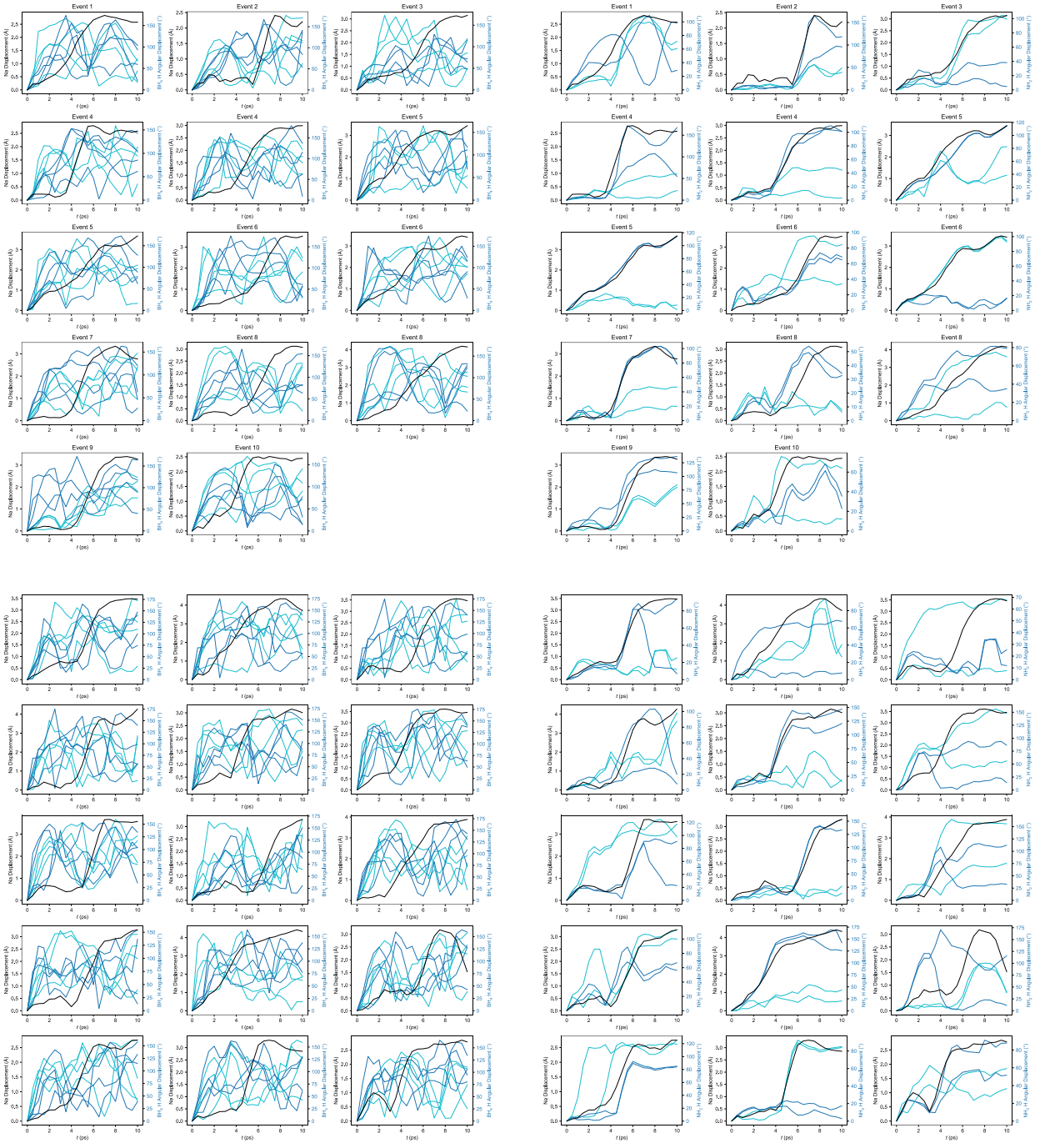
Event 1
Event 2
Event 3
Event 4
Event 4
Event 5
Event 5
Event 6
Event 6
Event 7
Event 8
Event 8
Event 9
Event 10
Na Displacement (Å)
BH3 H Angular Displacement (°)
NH3 H Angular Displacement (°)
t (ps)

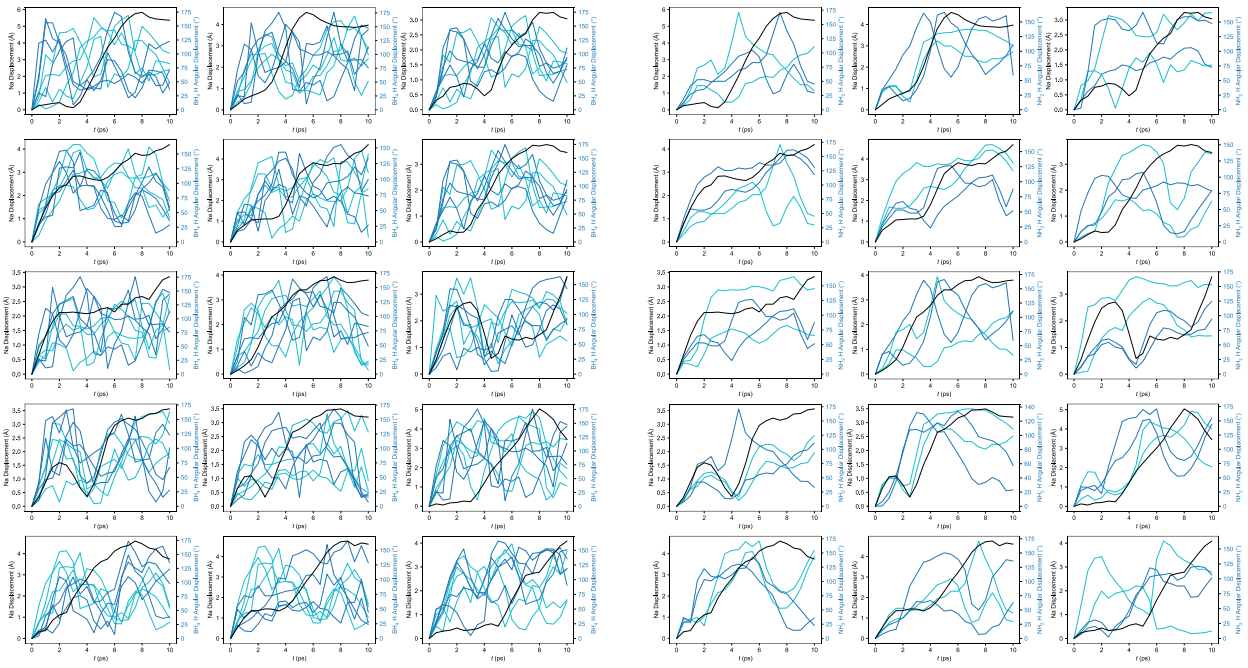

Figure S9. Correlation between sodium ion translation (left vertical axis, black line) and cluster anion angular displacement (right vertical axis, blue lines, the shade is indicative of which of the two nearest neighbors the hydrogen belongs to) plotted against time during a sampling of migration events in a 50 ps AIMD simulation of $Na_2(NH_2)(BH_4)$ at 363, 500, and 700 K (top to bottom).

NMR Results

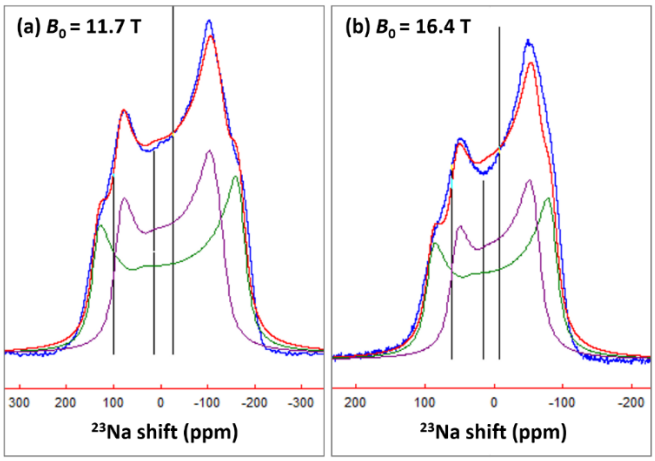

Figure S10. Spectral fits of ^{23}Na NMR spectra of orthorhombic $Na_2(NH_2)(BH_4)$, acquired at two different magnetic fields (B_0 = 11.7 T and 16.4 T), at 20 °C. The sample was previously cooled to obtain the orthorhombic phase, and then heated to 20 °C at which this phase was maintained due to the hysteretic phase transition. The two Na sites are depicted in purple ("axial" site) and green ("equatorial" site); the overall fit is shown in red and the experimental spectra are shown in blue. The fitted (C_Q, η_Q) values are (5.5 MHz, 0.1) and (6.8 MHz, 0.03) for the axial and equatorial Na sites, respectively; the corresponding DFT-calculated values for the orthorhombic crystal structure of $Na_2(NH_2)(BH_4)$ are (4.6 MHz, 0.26) and (6.7 MHz, 0.02).

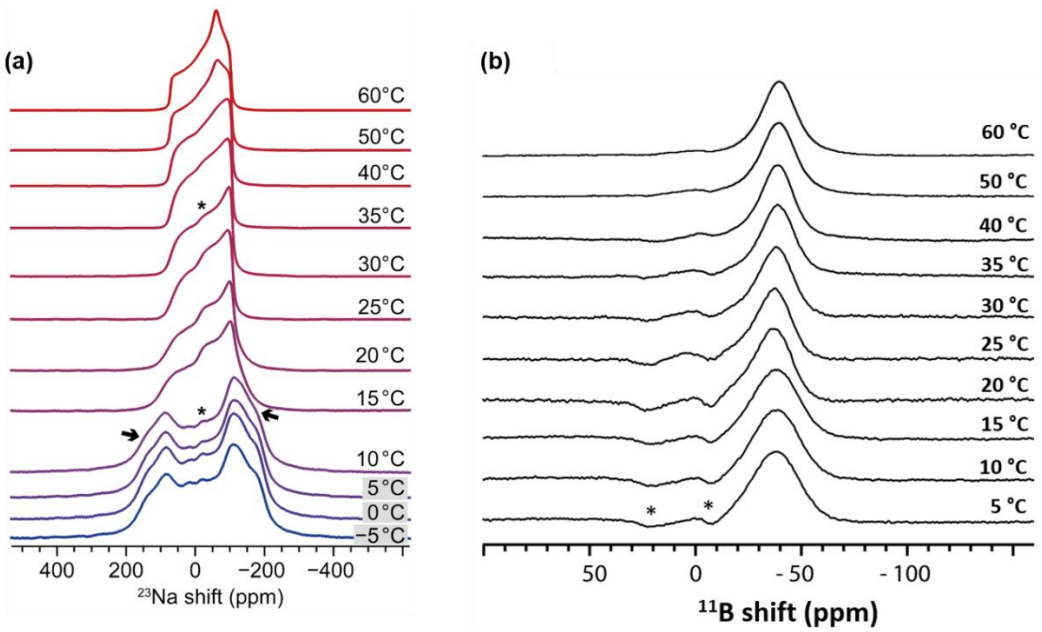

Figures S11. (A) Static variable-temperature ^{23}Na NMR of $Na_2(NH_2)(BH_4)$; spectra were obtained on cooling the sample after equilibrating at the highest temperature of 60 °C. The features arising from the appearance of the second ^{23}Na site in the orthorhombic phase, occurring at and below 10 °C, are indicated with arrows. Static variable-temperature ^{11}B NMR spectra of $Na_2(NH_2)(BH_4)$. Background signal arising from Na and B within the flame-sealed glass tube is indicated with an asterisk (*). The background signal for boron is inverted due to quadrupolar nutation effects.

Synthesis of $Na_{3-x}O_{1-x}(NH_2)_x(BH_4)$

x	Annealing Temperature (°C)
0	250
0.2	200
0.5	200
0.75	200
1	180
1, $^{11}BD_4$	100

Table S1. Annealing temperatures for various compositions of $Na_{3-x}O_{1-x}(NH_2)_x(BH_4)$.

R_{wp} = 1.05% Gof = 2.85						
S.G. *P*bcm a = 6.3448(19) Å b = 6.407(2) Å c = 9.789(2) Å						
Atom	Wyck.	*x*	*y*	*z*	Occ.	B_{eq} (Å^2)
Na1	8e	0.25	0.285(2)	0	0.53(1)	0.56(12)
Na2	4d	0.5783(12)	0.0783(12)	0.25	0.95(2)	0.56(12)
N	4d	0.25	0.25	0.25	1	0.14(4)
H1	4d	0.1452(5)	0.1452(5)	0.25	1	0.20(7)
H2	4d	0.1452(5)	0.3548(5)	0.25	1	0.20(7)
^{11}B	4c	0.75	0.25	0	1	0.81(9)
D1	8e	0.8622(4)	0.3622(4)	0.0673(5)	0.00(3)	5.00(12)
D2	8e	0.6378(4)	0.1378(4)	0.0673(5)	0.13(3)	5.00(12)
D3	8e	0.8622(4)	0.1378(4)	0.0673(5)	1.00(3)	5.00(12)
D4	8e	0.6378(4)	0.3622(4)	0.0673(5)	0.87(3)	5.00(12)

Table S2. Refined structure of $Na_2NH_2BD_4$ (100 K) from neutron diffraction data

	R_{wp} = 1.12% Gof = 3.27 S.G. *P*m-3m a = 4.6897(4) Å					
Atom	Wyck.	*x*	*y*	*z*	Occ.	B_{eq} (Å^2)
Na1	3d	0.5	0	0	0.67(2)	9.5(3)*
N1	1a	0	0	0	1	3.3(1)
H1	6e	0	0	0.2262(21)	0.333(6)	4.1(2)
^{11}B	1b	0.5	0.5	0.5	1	6.8(2)
D1	6f	0.5	0.5	0.2329(17)	0.446(7)	9.1(2)*
D2	8g	0.3571(18)	0.3571(18)	0.3571(18)	0.165(6)	9.1(2)*

Table S3. Refined structure of $Na_2NH_2BD_4$ (288 K) from neutron diffraction data. *Atomic displacement parameters are abnormally large, suggesting fast dynamics of these ions.